

Innovative Alphabet-Based Bayesian Compressive Sensing Technique for Imaging Targets with Arbitrary Shape

N. Alselmi, G. Oliveri, M. A. Hannan, M. Salucci, and A. Massa

Abstract

In this work an innovative two-dimensional ($2D$) microwave imaging technique exploiting Bayesian Compressive Sensing (BCS) and a wavelet-based *alphabet* for representing the problem unknowns is dealt with. The proposed approach is based on the generalization of the *sparsity* concept, extending the range of applicability of BCS -based inverse scattering (IS) techniques to objects with arbitrary shape and dimensions. A set of BCS reconstructions is performed considering different expansion bases in the alphabet, without the need for a-priori knowledge about the unknown scatterers. Then, the best reconstruction is recognized as that minimizing the number of non-null retrieved coefficients (i.e., the *sparsest* one). In order to verify the effectiveness of the proposed imaging technique, a set of representative numerical benchmarks is presented. Some comparisons with state-of-the-art IS techniques are presented, as well.

1 Numerical Results

1.1 Object Haar #0

GOAL: TO PROVE THE EFFECTIVENESS OF THE ALPHABET BASED APPROACH USING AN “AD-HOC” SCATTERER FOR HAAR WAVELETS.

Test Case Description

Object:

- $\varepsilon_{r,max} = 1.01$
- $\sigma = 0$ [S/m]
- Number of Haar coefficients: $N_C = 2$

Sources:

- Plane waves
- Amplitude: $A = 1$
- Frequency: 300 MHz ($\lambda = 1\text{m}$)
- Number of views: $V = 36$

Direct solver:

- Square domain divided in $\sqrt{D} \times \sqrt{D}$ cells
- $D = 4096$ (64×64) ($\frac{L_D}{\sqrt{D}} = \frac{\lambda}{16}$)

Investigation domain:

- Square domain divided in $\sqrt{N} \times \sqrt{N}$ cells
- $N = 1024$ (32×32) ($\frac{L_D}{\sqrt{N}} = \frac{\lambda}{8}$)
- $L_D = 4\lambda$

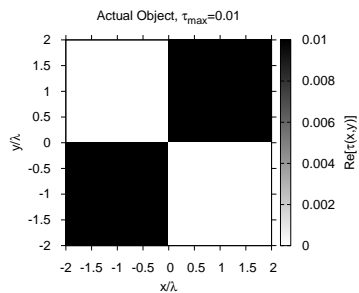
Measurement domain:

- Measurement points taken on a circle of radius $\rho = 4\lambda$
- $M = 36$

M-BCS parameters:

- $a = 1.0 \times 10^{-2}$
- $b = 1.0 \times 10^{-5}$

ACTUAL

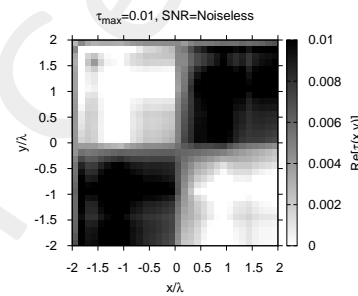
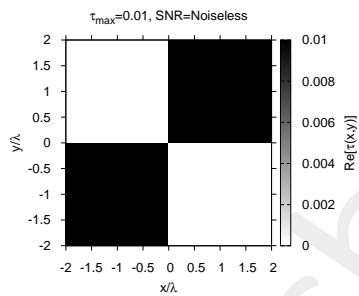
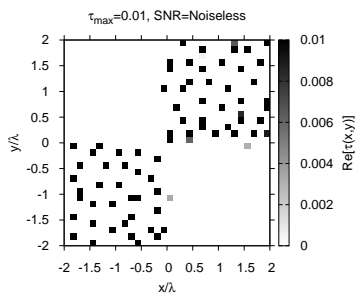


PIXEL

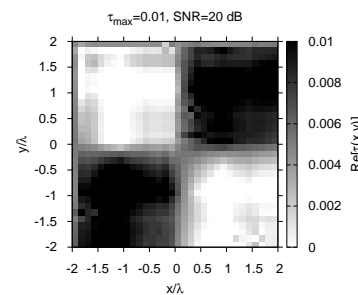
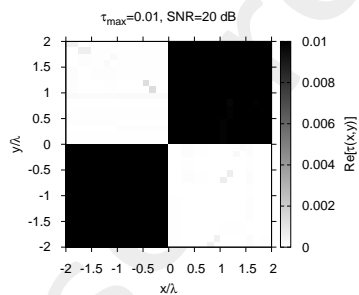
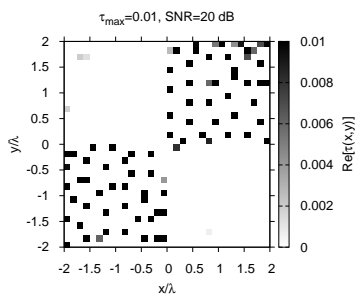
HAAR

DAUB4

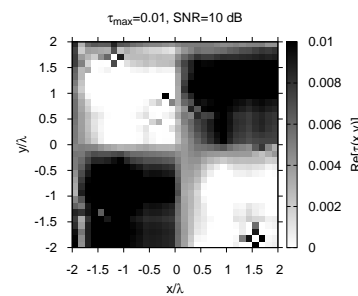
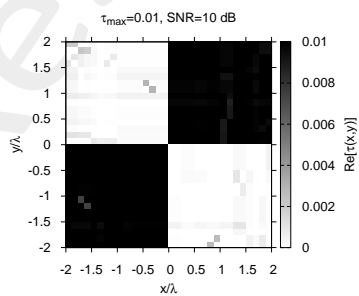
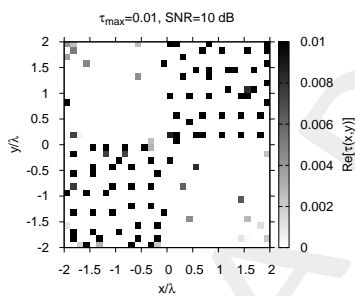
NOISELESS



SNR=20 dB



SNR=10 dB



SNR=5 dB

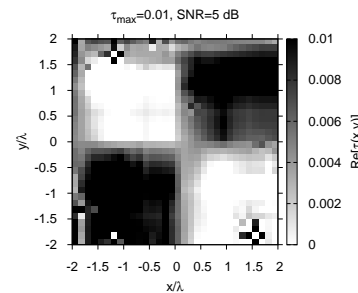
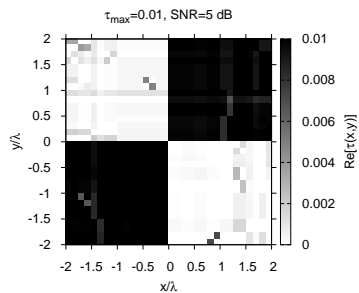
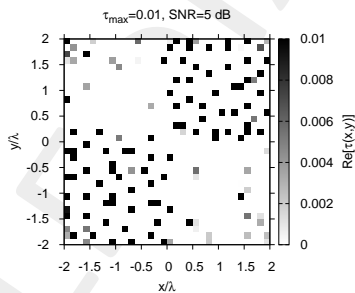
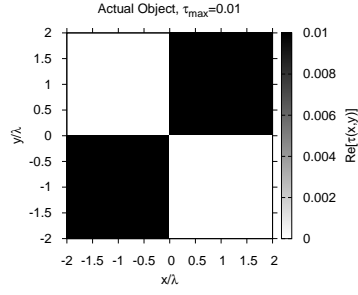


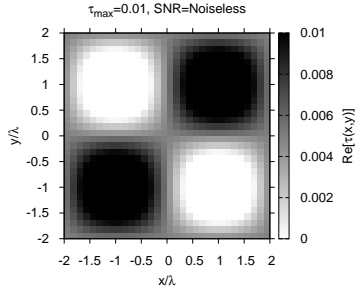
Figure 1: Actual and retrieved object (real part) considering different wavelet expansions.

ACTUAL

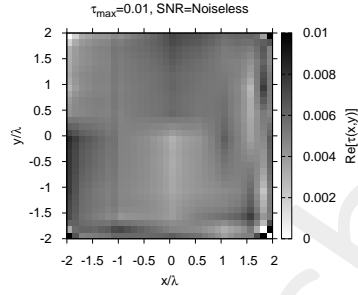


NOISELESS

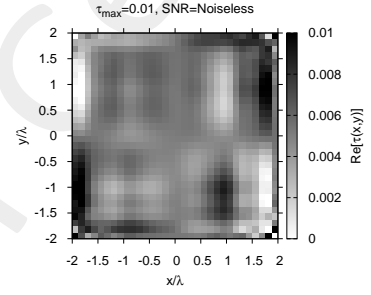
EXP



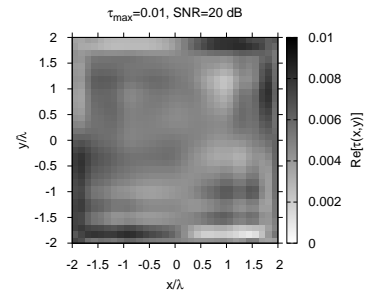
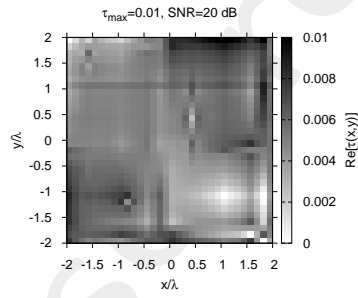
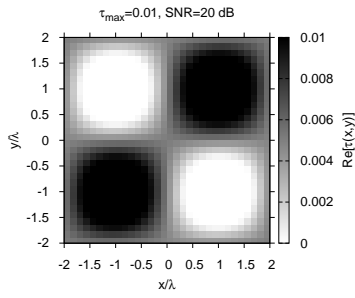
COIF



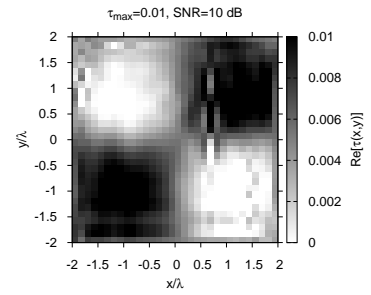
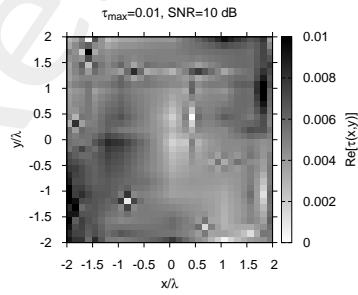
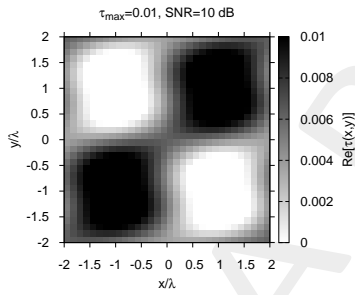
DMEY



SNR=20 dB



SNR=10 dB



SNR=5 dB

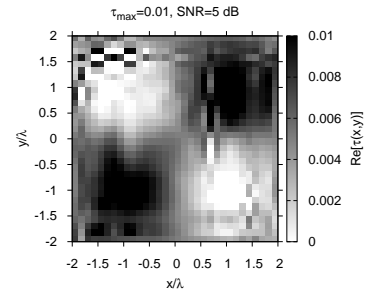
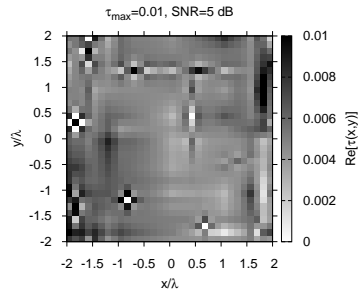
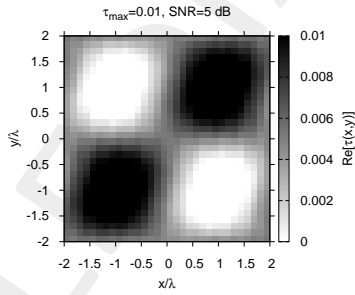
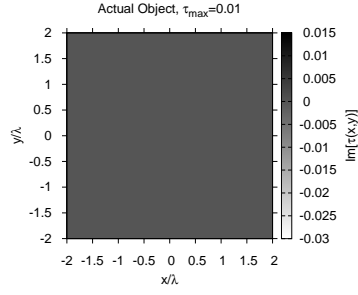


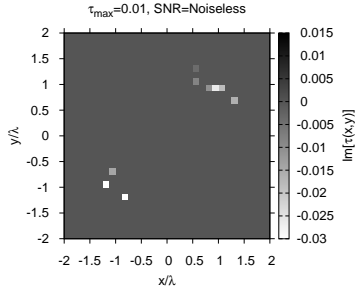
Figure 2: Actual and retrieved object considering different wavelet expansions.

ACTUAL

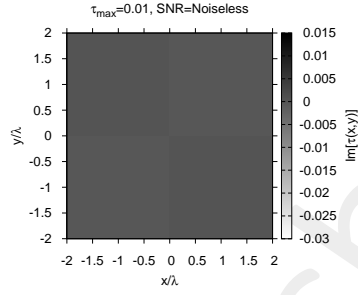


NOISELESS

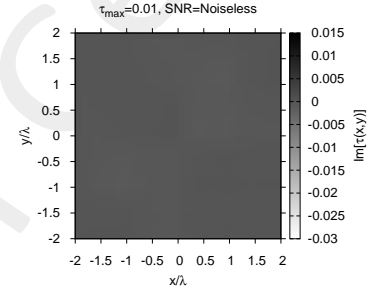
PIXEL



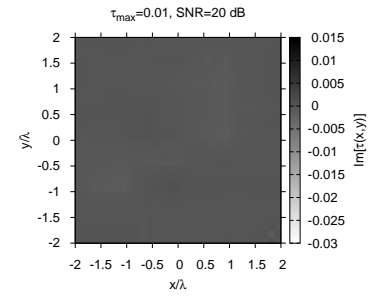
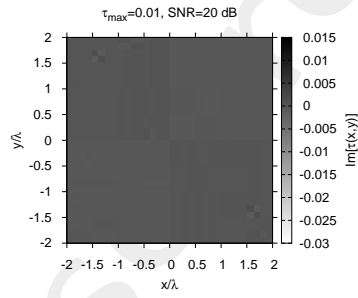
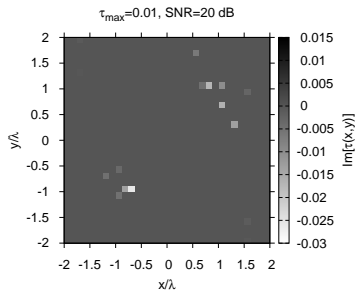
HAAR



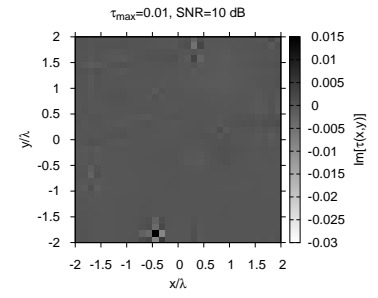
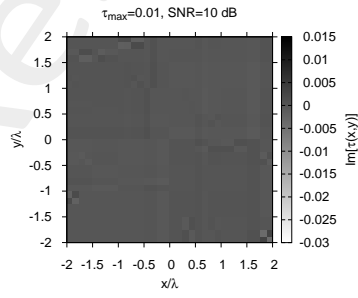
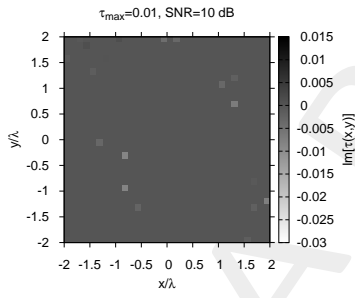
DAUB4



SNR=20 dB



SNR=10 dB



SNR=5 dB

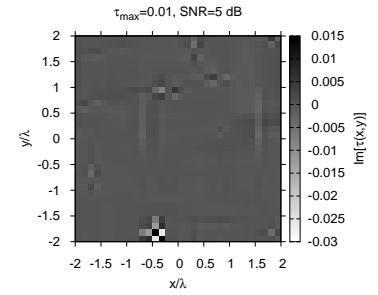
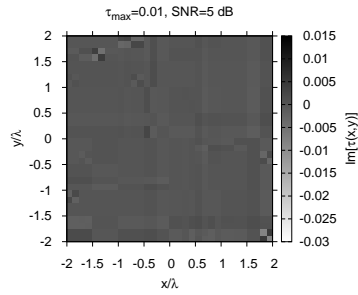
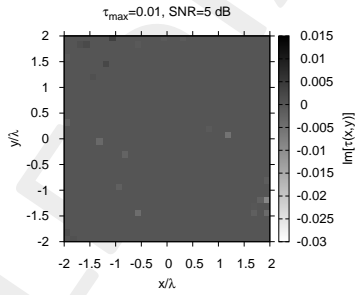
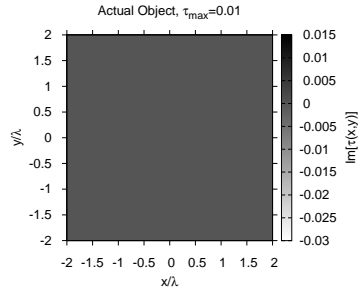


Figure 3: Actual and retrieved object (imaginary part) considering different wavelet expansions.

ACTUAL

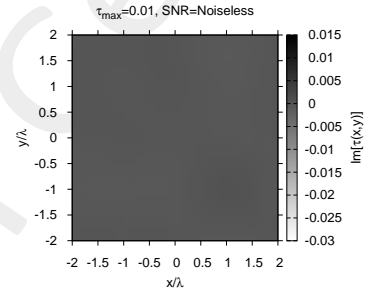
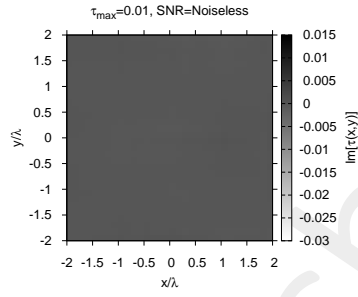
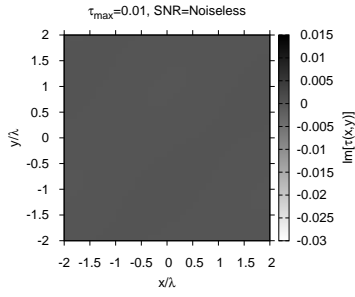


EXP

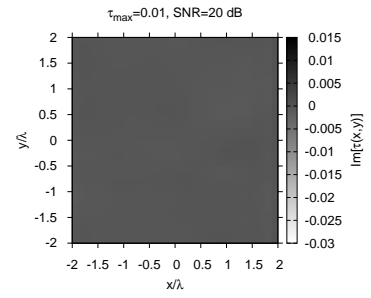
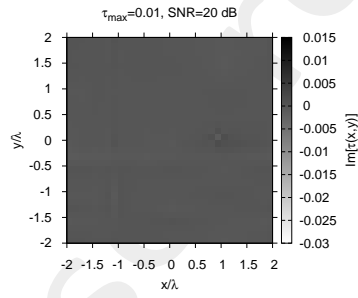
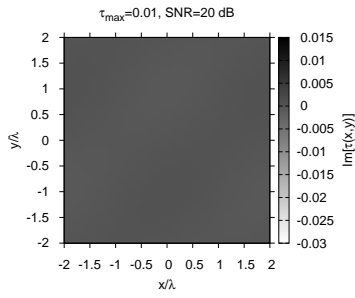
COIF

DMEY

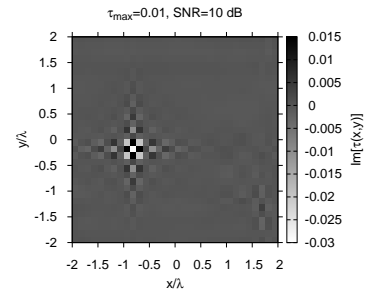
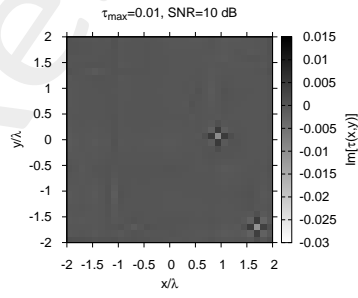
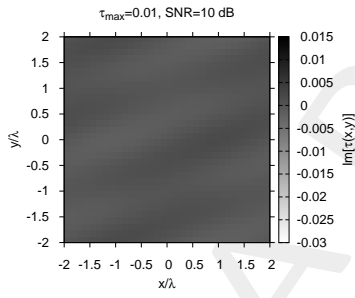
NOISELESS



SNR=20 dB



SNR=10 dB



SNR=5 dB

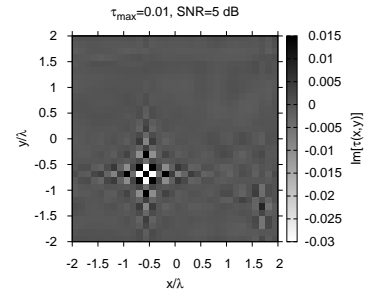
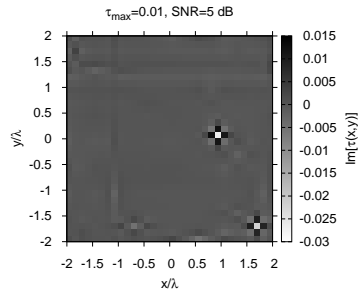
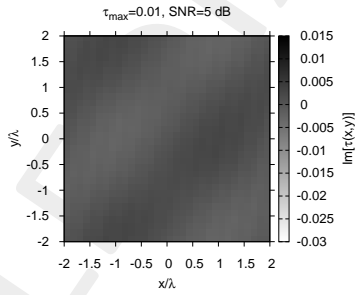


Figure 4: Actual and retrieved object considering different wavelet expansions.

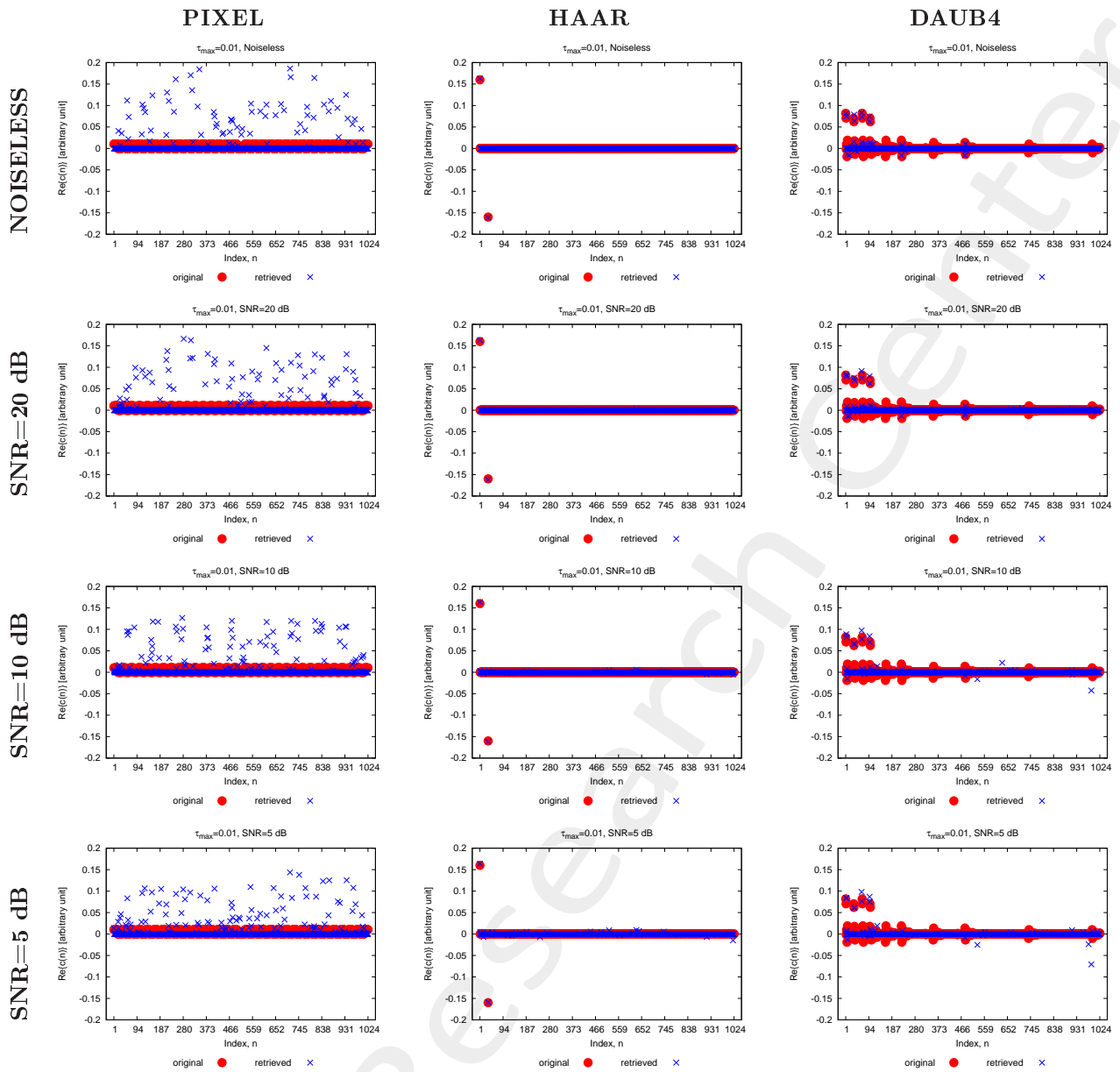


Figure 5: Real part of the actual and retrieved coefficients considering different wavelet expansions.

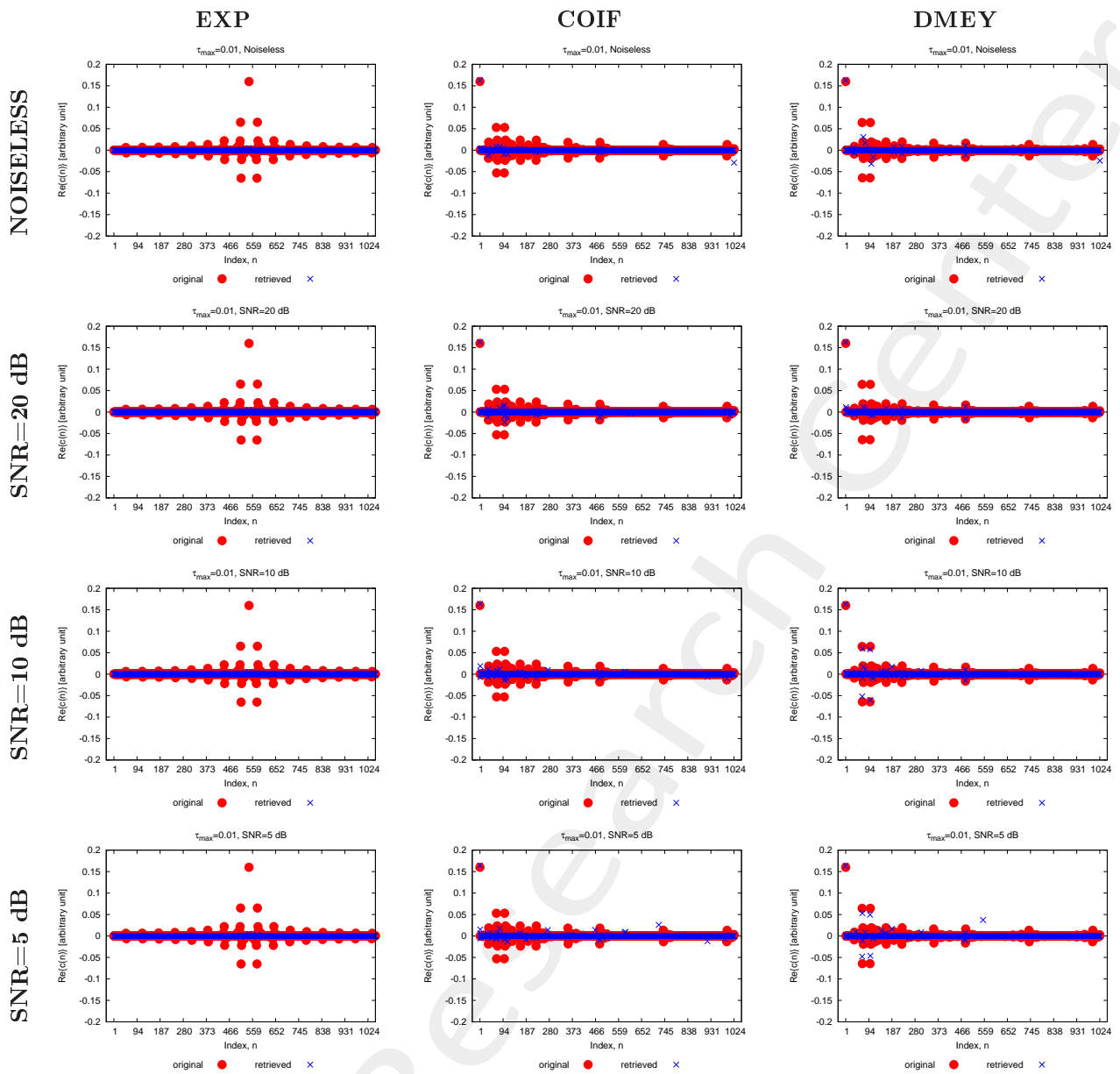


Figure 6: Real part of the actual and retrieved coefficients considering different wavelet expansions.

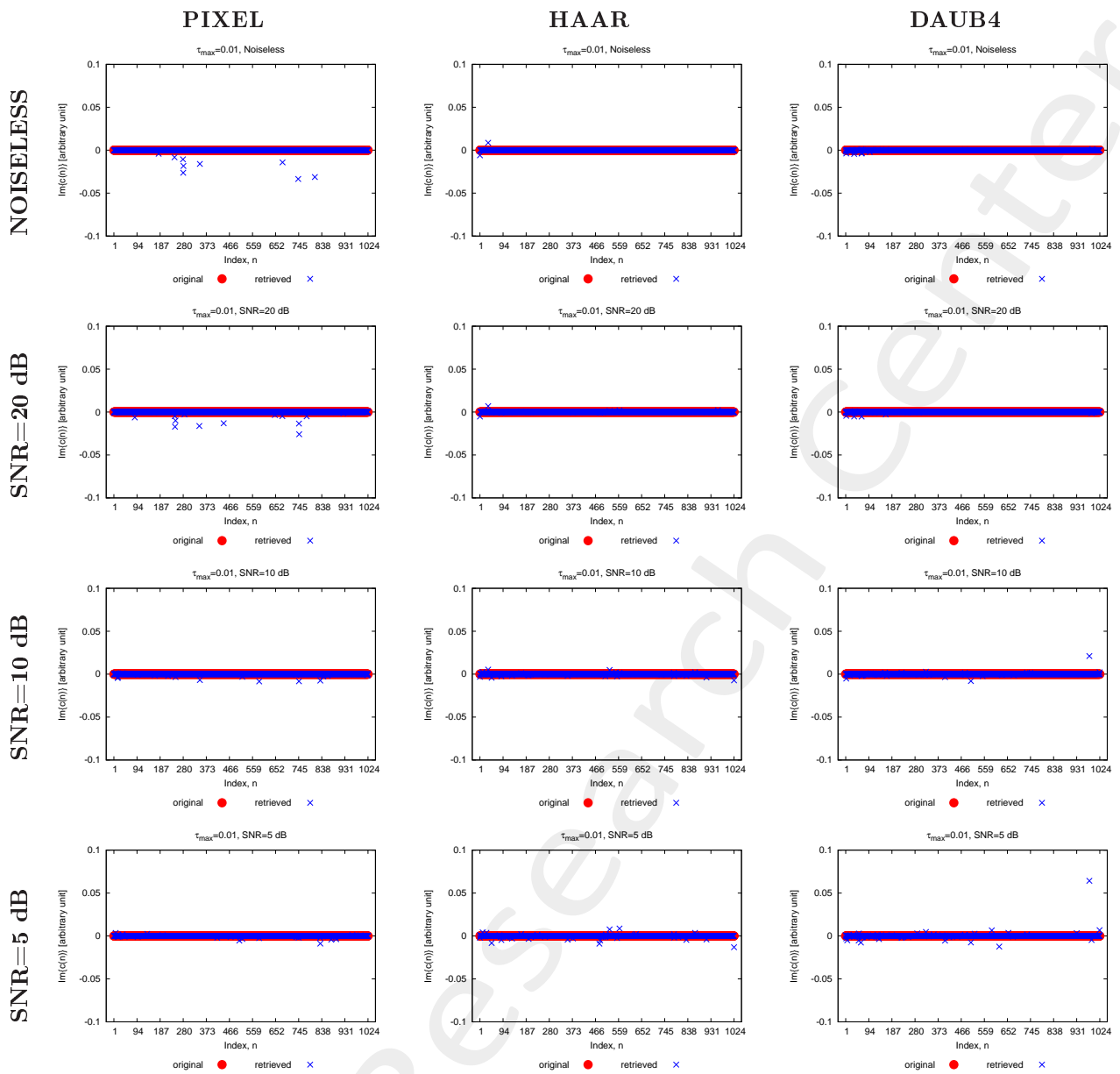


Figure 7: Imaginary part of the actual and retrieved coefficients considering different wavelet expansions.

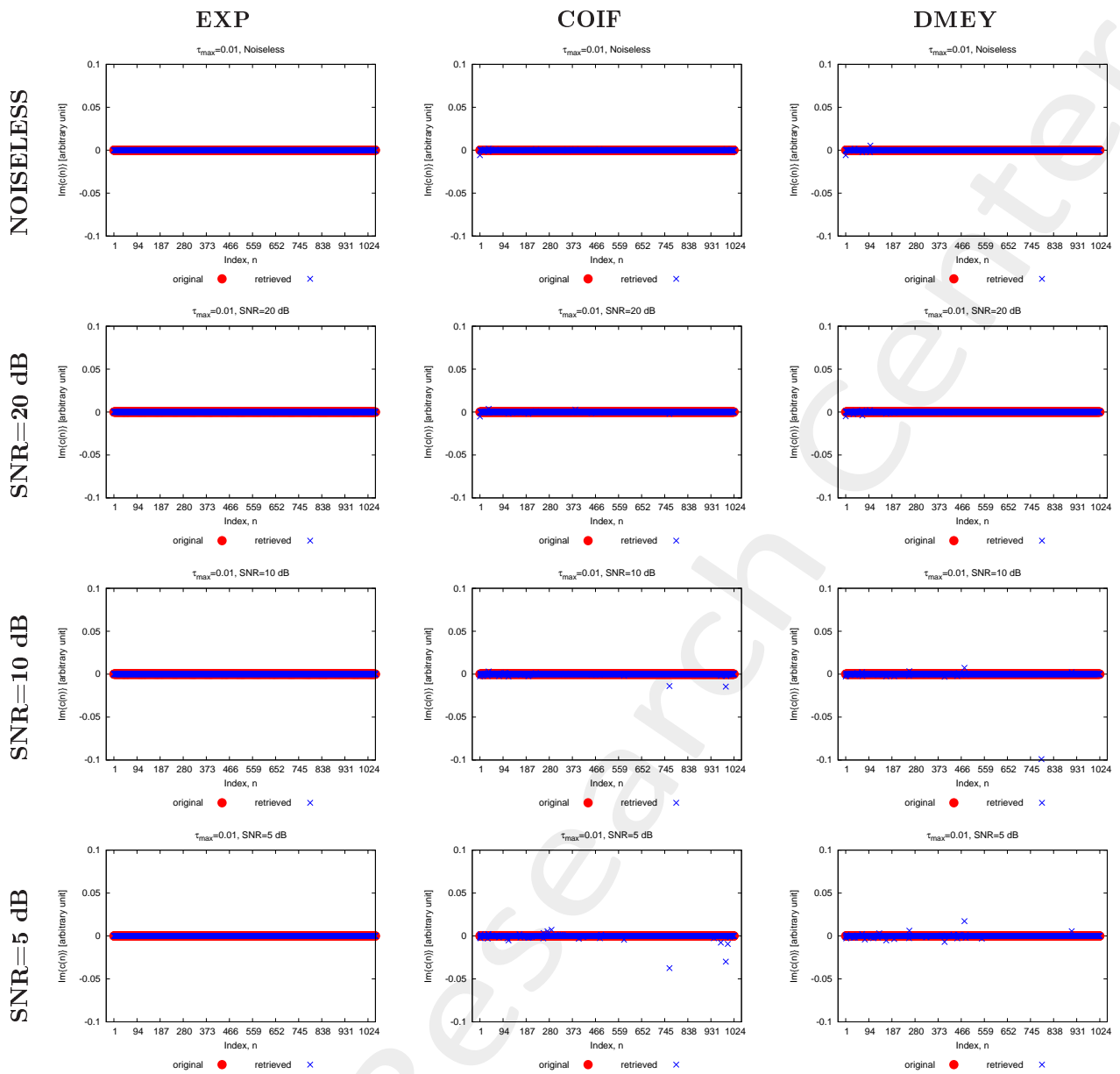


Figure 8: Imaginary part of the actual and retrieved coefficients considering different wavelet expansions.

Coefficients Analysis $T = 100\%$:

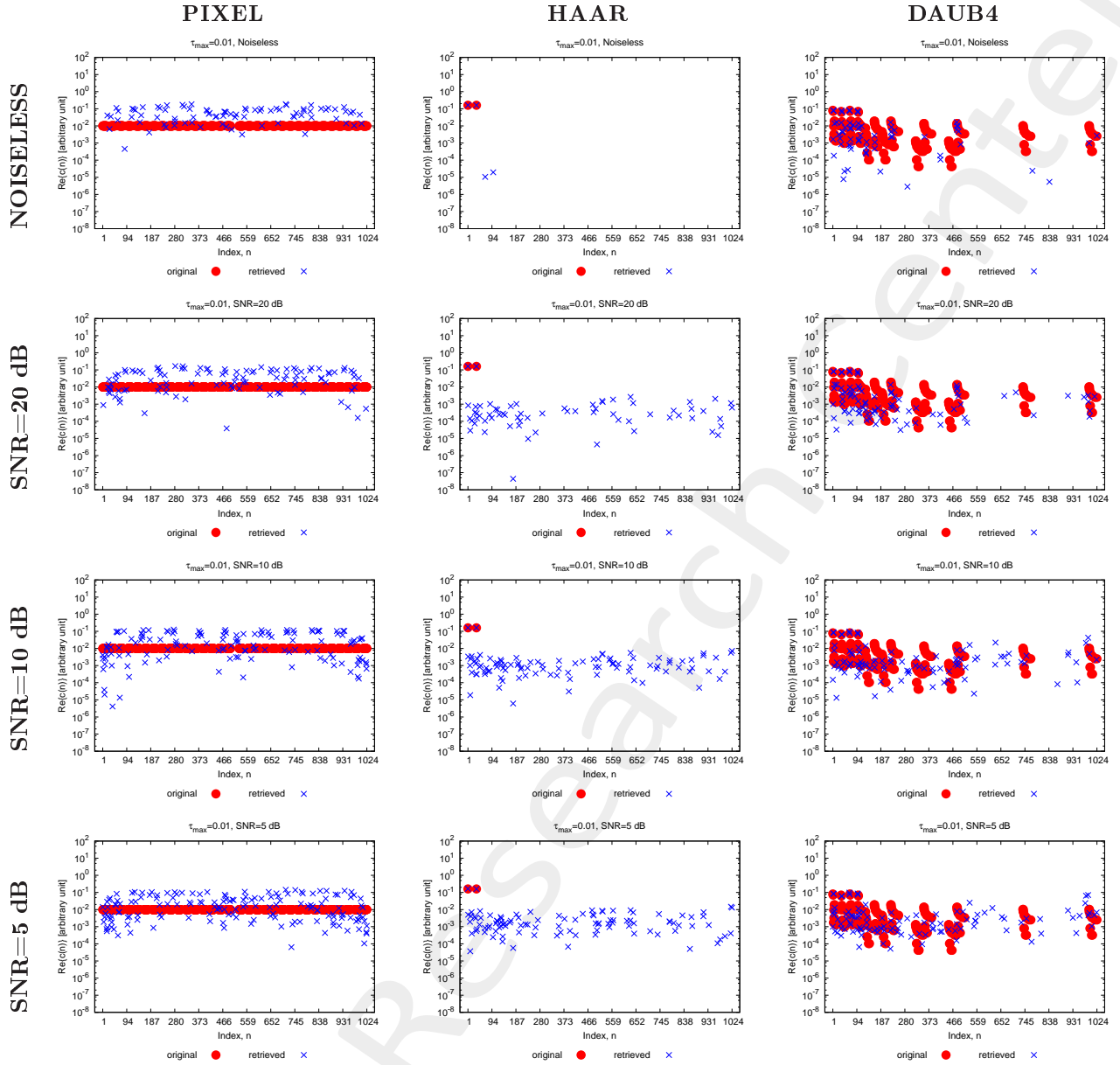


Figure 9: Absolute value (dB) of the actual and retrieved coefficients considering different wavelet expansions.

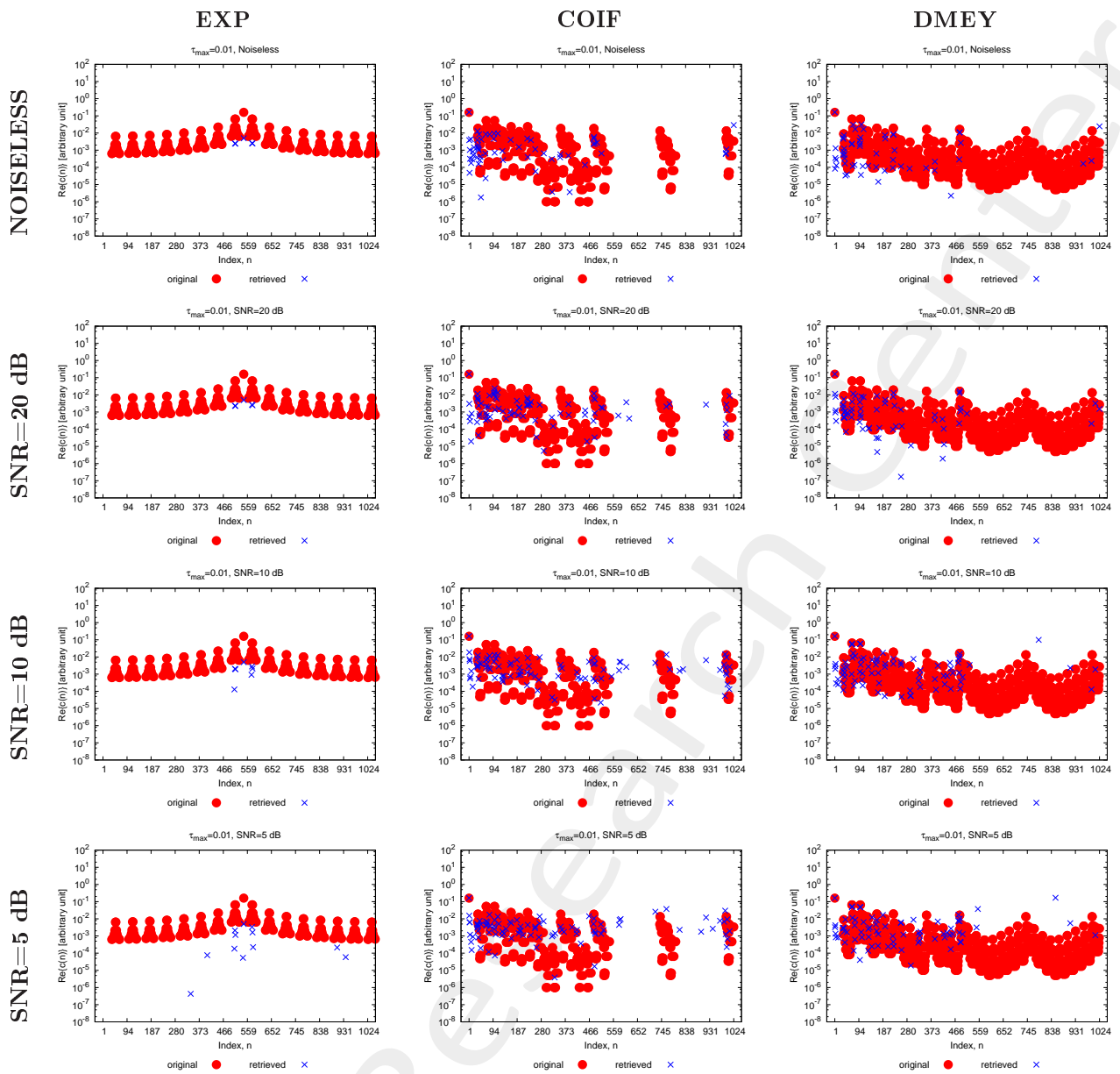


Figure 10: Absolute value (dB) of the actual and retrieved coefficients considering different wavelet expansions.

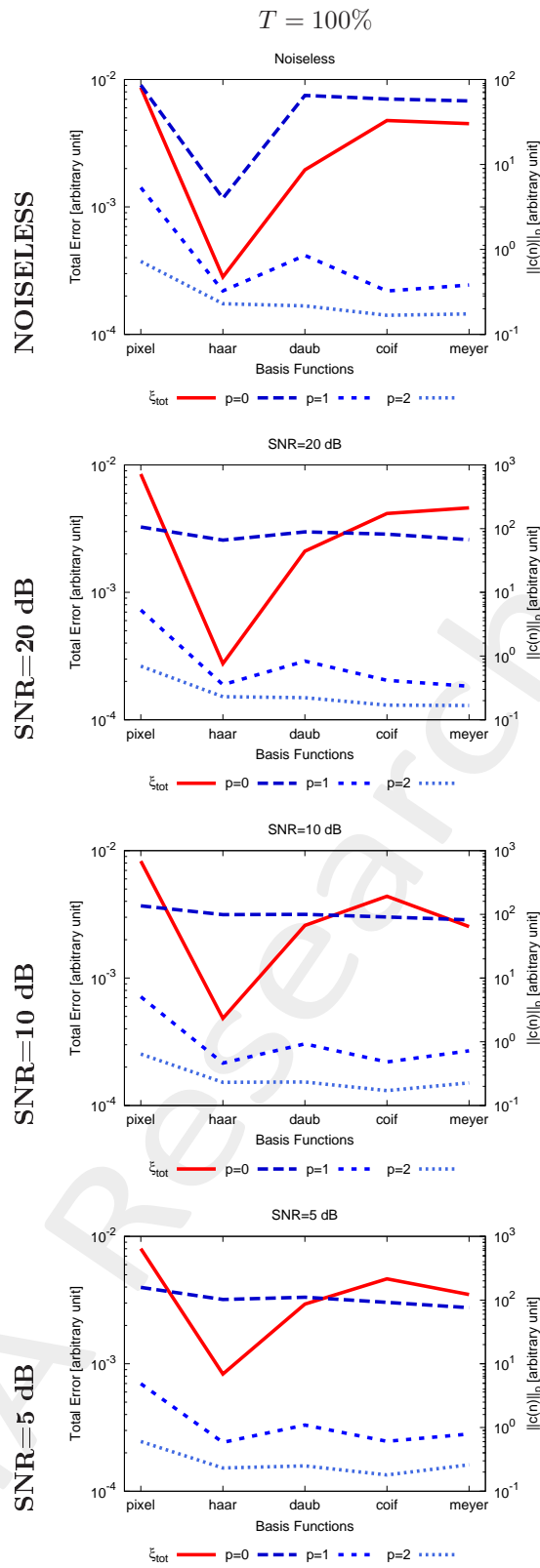


Figure 11: $[T = 100\%]$ - Comparison of ξ_{tot} , and L_0, L_1, L_2 Norms of the retrieved basis expansion coefficients, for each alphabet basis.

$L_0 - norm$						
SNR [dB]	$Pixel$	$Haar$	$Daub4$	$Coiflet$	$DMeyer$	Exp
<i>Actual</i>	512	2	196	358	962	241
<i>Noiseless</i>	86	4	65	49	56	5
20	106	66	89	89	82	5
10	136	99	100	91	82	7
5	158	102	111	92	76	12
$L_1 - norm$						
SNR [dB]	$Pixel$	$Haar$	$Daub4$	$Coiflet$	$DMeyer$	Exp
<i>Actual</i>	163.8	0.32	1.53	1.60	1.50	1.32
<i>Noiseless</i>	5.34	0.32	0.85	0.32	0.38	1.5×10^{-2}
20	5.28	0.35	0.83	0.42	0.33	1.5×10^{-2}
10	5.09	0.46	0.93	0.48	0.72	1.5×10^{-2}
5	4.87	0.58	1.09	0.61	0.79	1.4×10^{-2}
$L_2 - norm$						
SNR [dB]	$Pixel$	$Haar$	$Daub4$	$Coiflet$	$DMeyer$	Exp
<i>Actual</i>	7.24	0.23	0.23	0.23	0.23	0.23
<i>Noiseless</i>	0.72	0.23	0.22	0.20	0.17	7.0×10^{-3}
20	0.69	0.23	0.22	0.17	0.16	6.9×10^{-3}
10	0.64	0.23	0.23	0.17	0.22	6.8×10^{-3}
5	0.60	0.23	0.24	0.18	0.26	6.7×10^{-3}

Table 1: [$T = 100\%$] - Number of the retrieved non-zero coefficients ($L_0 - norm$), $L_1 - norm$, and $L_2 - norm$ using different wavelet functions.

Thresholded Analysis:

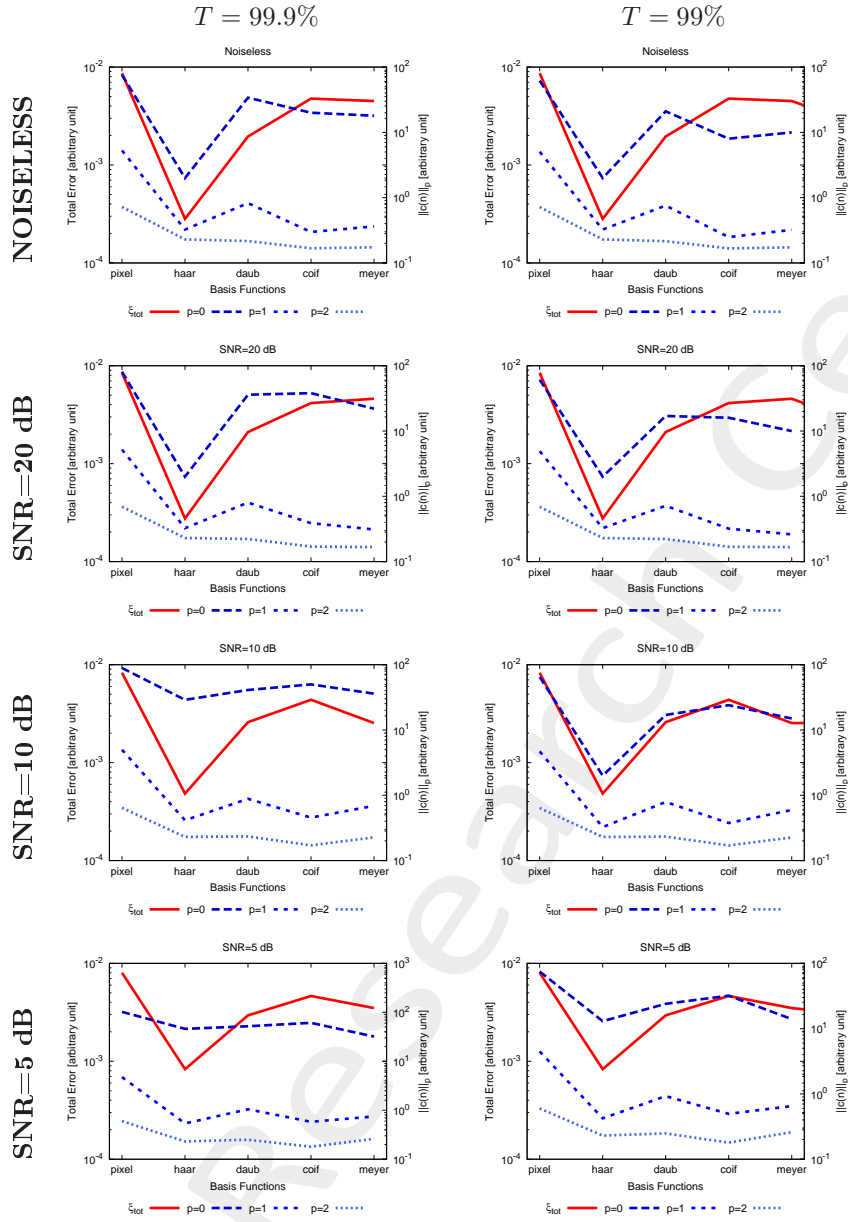


Figure 12: Comparison of ξ_{tot} , and L_0, L_1, L_2 Norms of the retrieved basis expansion coefficients, for each alphabet basis.

$L_0 - norm$					
SNR [dB]	<i>Pixel</i>	<i>Haar</i>	<i>Daub4</i>	<i>Coiflet</i>	<i>DMeyer</i>
<i>Actual</i>	512	2	196	358	962
<i>Noiseless</i>	76	2	34	20	18
20	81	2	36	38	22
10	89	29	41	50	36
5	102	46	52	61	32
$L_1 - norm$					
SNR [dB]	<i>Pixel</i>	<i>Haar</i>	<i>Daub4</i>	<i>Coiflet</i>	<i>DMeyer</i>
<i>Actual</i>	163.8	0.32	1.53	1.60	1.50
<i>Noiseless</i>	5.28	0.32	0.82	0.30	0.36
20	5.20	0.33	0.80	0.39	0.31
10	4.98	0.41	0.88	0.45	0.69
5	4.75	0.54	1.04	0.58	0.75
$L_2 - norm$					
SNR [dB]	<i>Pixel</i>	<i>Haar</i>	<i>Daub4</i>	<i>Coiflet</i>	<i>DMeyer</i>
<i>Actual</i>	7.24	0.23	0.23	0.23	0.23
<i>Noiseless</i>	0.72	0.23	0.22	0.17	0.17
20	0.69	0.23	0.22	0.17	0.17
10	0.64	0.23	0.23	0.17	0.23
5	0.60	0.23	0.25	0.18	0.26

Table 2: $[T = 99.9\%]$ - Number of the retrieved non-zero coefficients ($L_0 - norm$), $L_1 - norm$, and $L_2 - norm$ using different wavelet functions.

$L_0 - norm$					
SNR [dB]	<i>Pixel</i>	<i>Haar</i>	<i>Daub4</i>	<i>Coiflet</i>	<i>DMeyer</i>
<i>Actual</i>	512	2	196	358	962
<i>Noiseless</i>	62	2	21	8	10
20	61	2	17	16	10
10	65	2	17	24	15
5	75	13	24	32	14
$L_1 - norm$					
SNR [dB]	<i>Pixel</i>	<i>Haar</i>	<i>Daub4</i>	<i>Coiflet</i>	<i>DMeyer</i>
<i>Actual</i>	163.8	0.32	1.53	1.60	1.50
<i>Noiseless</i>	5.06	0.32	0.76	0.25	0.32
20	4.92	0.33	0.72	0.32	0.26
10	4.71	0.33	0.79	0.38	0.60
5	4.48	0.42	0.93	0.50	0.65
$L_2 - norm$					
SNR [dB]	<i>Pixel</i>	<i>Haar</i>	<i>Daub4</i>	<i>Coiflet</i>	<i>DMeyer</i>
<i>Actual</i>	7.24	0.23	0.23	0.23	0.23
<i>Noiseless</i>	0.72	0.23	0.22	0.17	0.17
20	0.69	0.23	0.22	0.17	0.17
10	0.64	0.23	0.23	0.17	0.23
5	0.60	0.23	0.25	0.18	0.26

Table 3: $[T = 99\%]$ - Number of the retrieved non-zero coefficients ($L_0 - norm$), $L_1 - norm$, and $L_2 - norm$ using different wavelet functions.

Resume:

$T = 100\%$					
SNR [dB]	<i>Pixel</i>	<i>Haar</i>	<i>Daub4</i>	<i>Coiflet</i>	<i>DMeyer</i>
<i>Noiseless</i>	86	4	65	49	56
20	106	66	89	89	82
10	136	99	100	91	82
5	158	102	111	92	76
$T = 99.9\%$					
SNR [dB]	<i>Pixel</i>	<i>Haar</i>	<i>Daub4</i>	<i>Coiflet</i>	<i>DMeyer</i>
<i>Noiseless</i>	76	2	34	20	18
20	81	2	36	38	22
10	89	29	41	50	36
5	102	46	52	61	32
$T = 99\%$					
SNR [dB]	<i>Pixel</i>	<i>Haar</i>	<i>Daub4</i>	<i>Coiflet</i>	<i>DMeyer</i>
<i>Noiseless</i>	62	2	21	8	10
20	61	2	17	16	10
10	65	2	17	24	15
5	75	13	24	32	14

Table 4: L_0 – norm.

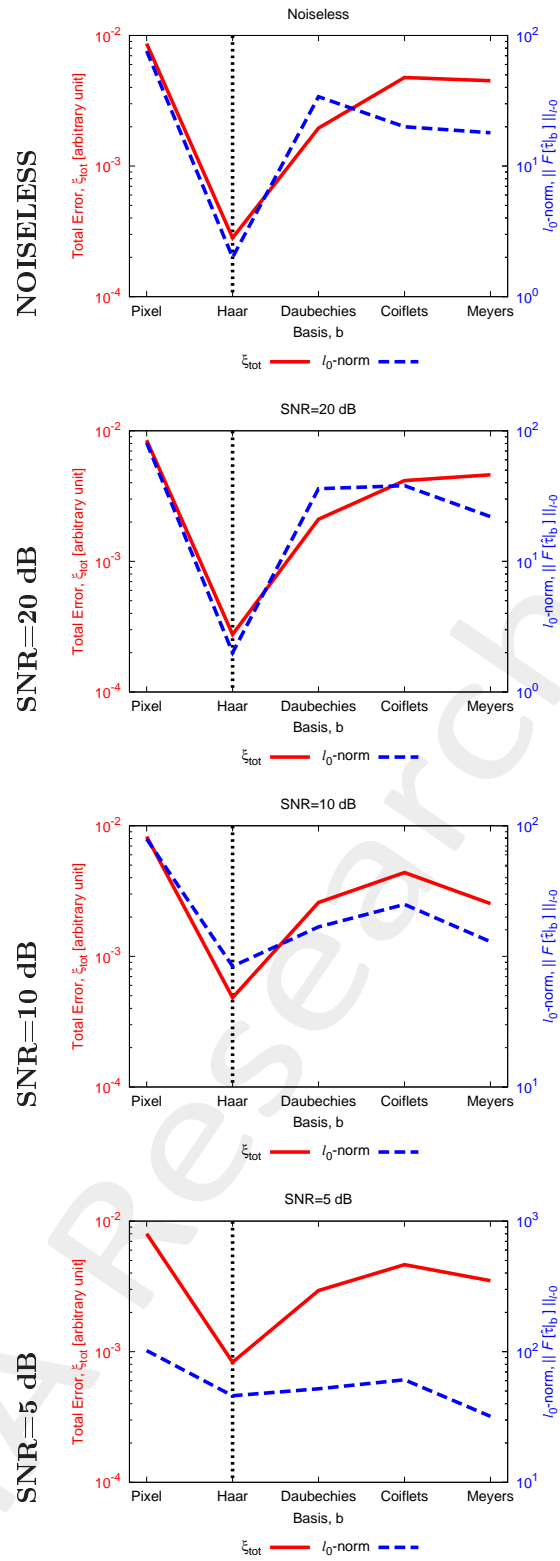
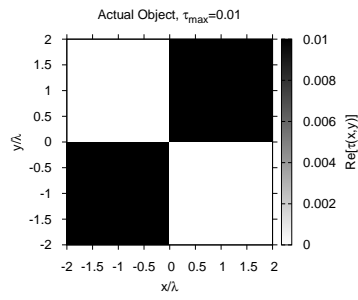


Figure 13: L_0 - norm vs Total Error, considering $T = 99.9\%$.

Comparison SoA

ACTUAL

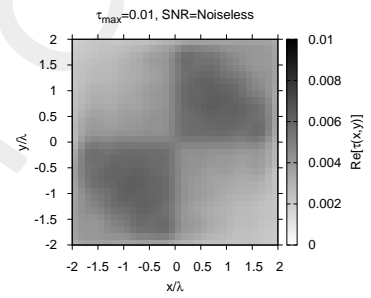
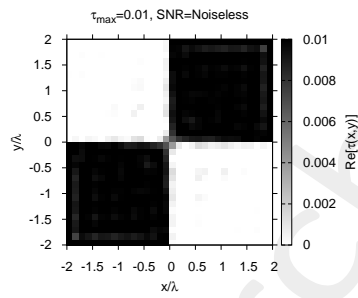
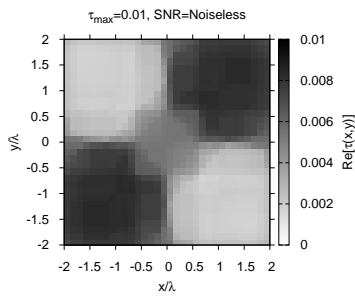


TV

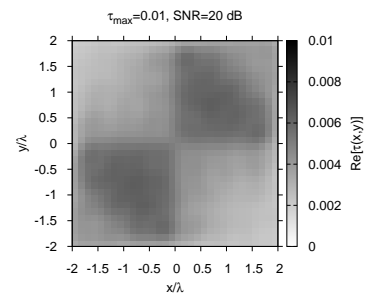
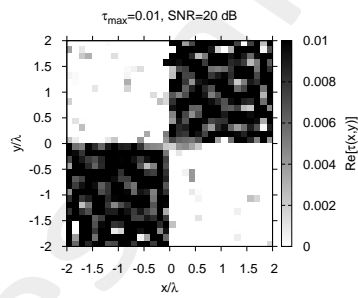
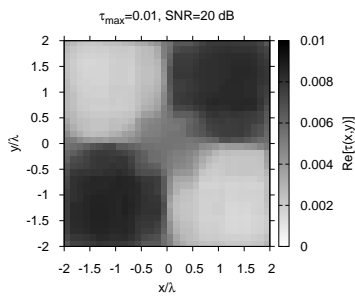
CG

SVD

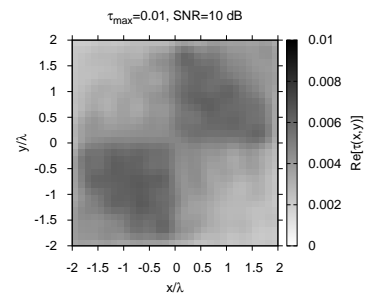
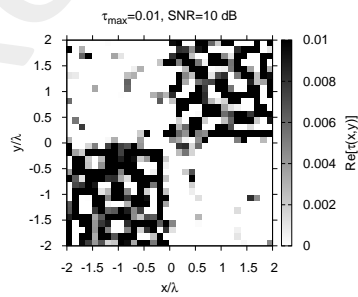
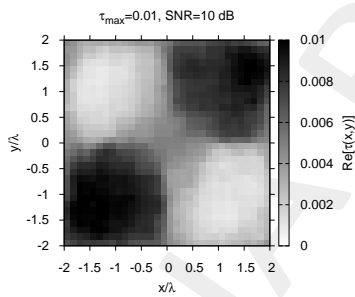
NOISELESS



SNR=20 dB



SNR=10 dB



SNR=5 dB

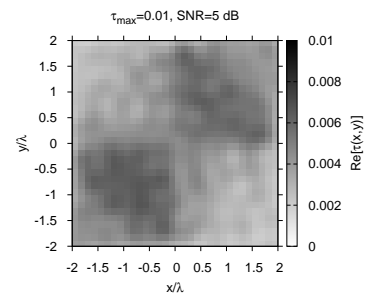
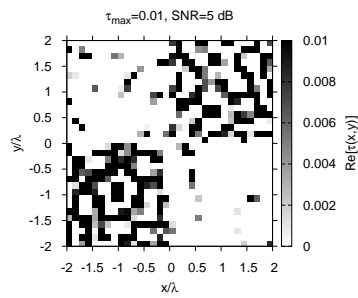
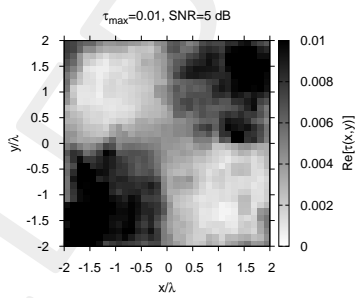
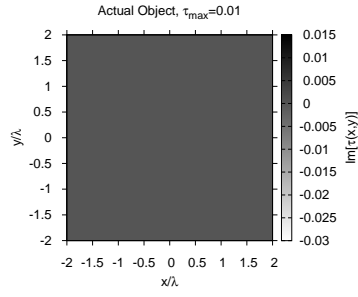
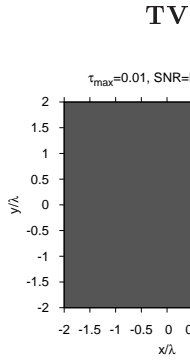


Figure 14: Actual and retrieved object considering different wavelet expansions.

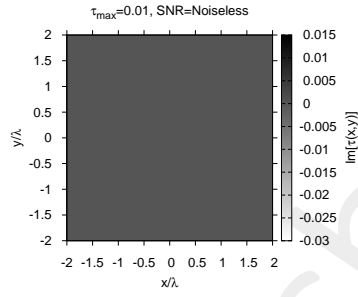
ACTUAL



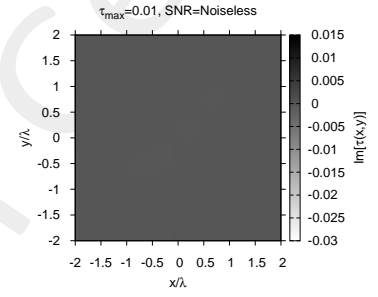
NOISELESS



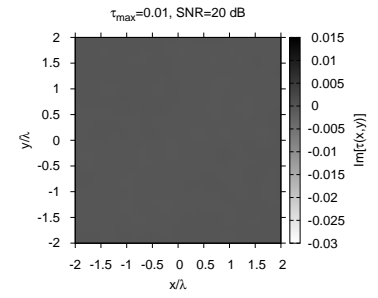
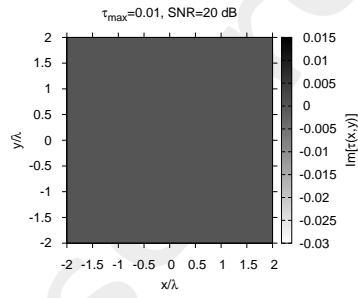
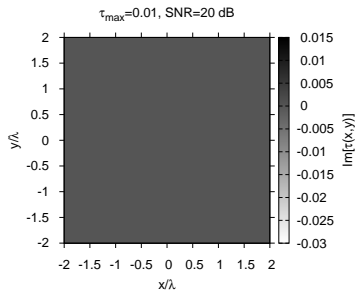
CG



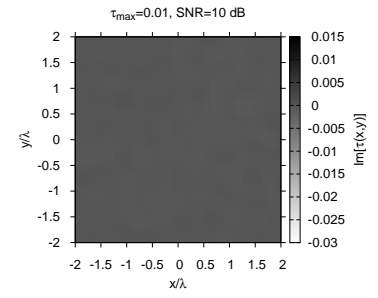
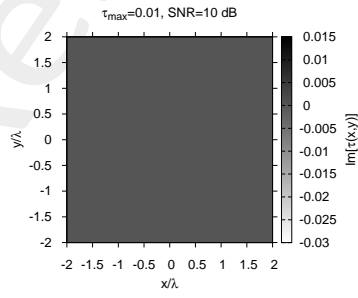
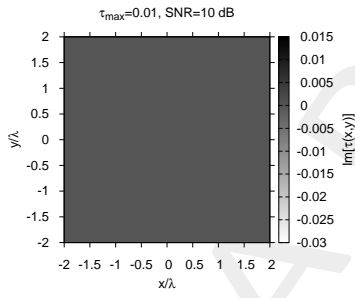
SVD



SNR=20 dB



SNR=10 dB



SNR=5 dB

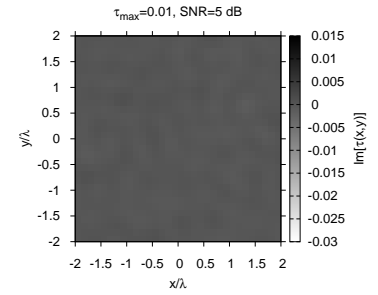
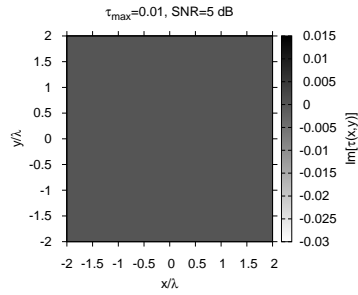
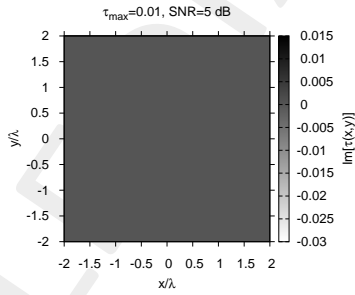


Figure 15: Actual and retrieved object considering different wavelet expansions.

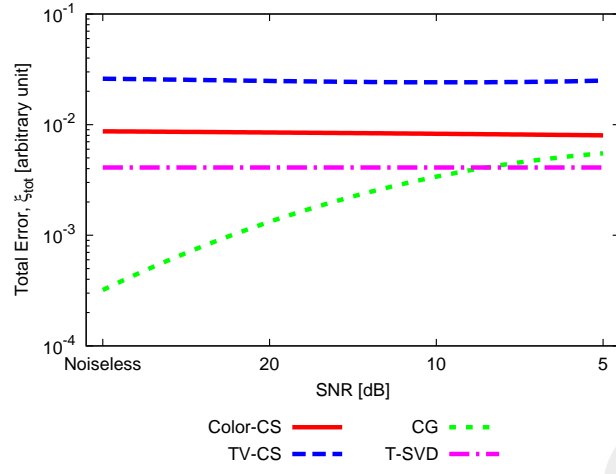


Figure 16: Comparison with SoA - Total Error vs SNR , considering $T = 99.9\%$.

SNR [dB]	TV [s]	CG [s]	SVD [s]	ALPHABET [s]
<i>Noiseless</i>	3.9×10^2	6.9×10^3	3.3×10^1	9.5×10^2
20	3.7×10^2	5.8×10^3	3.4×10^1	1.0×10^3
10	3.8×10^2	6.1×10^3	3.5×10^1	8.7×10^2
5	3.9×10^2	5.7×10^3	3.5×10^1	8.5×10^2

Table 5: Timings.

References

- [1] A. Massa, P. Rocca, and G. Oliveri, "Compressive sensing in electromagnetics - A review," *IEEE Antennas Propag. Mag.*, pp. 224-238, vol. 57, no. 1, Feb. 2015.
- [2] A. Massa and F. Teixeira, Guest-Editorial: Special Cluster on Compressive Sensing as Applied to Electromagnetics, *IEEE Antennas Wireless Propag. Lett.*, vol. 14, pp. 1022-1026, 2015.
- [3] G. Oliveri, N. Anselmi, and A. Massa, "Compressive sensing imaging of non-sparse 2D scatterers by a total-variation approach within the Born approximation," *IEEE Trans. Antennas Propag.*, vol. 62, no. 10, pp. 5157-5170, Oct. 2014.
- [4] L. Poli, G. Oliveri, and A. Massa, "Imaging sparse metallic cylinders through a Local Shape Function Bayesian Compressive Sensing approach," *J. Opt. Soc. Am. A*, vol. 30, no. 6, pp. 1261-1272, 2013.
- [5] F. Viani, L. Poli, G. Oliveri, F. Robol, and A. Massa, "Sparse scatterers imaging through approximated multitask compressive sensing strategies," *Microwave Opt. Technol. Lett.*, vol. 55, no. 7, pp. 1553-1558, Jul. 2013.
- [6] M. Salucci, G. Oliveri, and A. Massa, "GPR prospecting through an inverse scattering frequency-hopping multi-focusing approach," *IEEE Trans. Geosci. Remote Sens.*, vol. 53, no. 12, pp. 6573-6592, Dec. 2015.
- [7] M. Salucci, L. Poli, N. Anselmi and A. Massa, "Multifrequency particle swarm optimization for enhanced multiresolution GPR microwave imaging," *IEEE Trans. Geosci. Remote Sens.*, vol. 55, no. 3, pp. 1305-1317, Mar. 2017.
- [8] M. Salucci, L. Poli, and A. Massa, "Advanced multi-frequency GPR data processing for non-linear deterministic imaging," Signal Processing - Special Issue on 'Advanced Ground-Penetrating Radar Signal-Processing Techniques,' vol. 132, pp. 306-318, March 2017.
- [9] L. Poli, G. Oliveri, P. Rocca, and A. Massa, "Bayesian compressive sensing approaches for the reconstruction of two-dimensional sparse scatterers under TE illumination," *IEEE Trans. Geosci. Remote Sens.*, vol. 51, no. 5, pp. 2920-2936, May 2013.
- [10] L. Poli, G. Oliveri, and A. Massa, "Microwave imaging within the first-order Born approximation by means of the contrast-field Bayesian compressive sensing," *IEEE Trans. Antennas Propag.*, vol. 60, no. 6, pp. 2865-2879, Jun. 2012.
- [11] G. Oliveri, P. Rocca, and A. Massa, "A bayesian compressive sampling-based inversion for imaging sparse scatterers," *IEEE Trans. Geosci. Remote Sens.*, vol. 49, no. 10, pp. 3993-4006, Oct. 2011.
- [12] G. Oliveri, L. Poli, P. Rocca, and A. Massa, "Bayesian compressive optical imaging within the Rytov approximation," *Optics Letters*, vol. 37, no. 10, pp. 1760-1762, 2012.

- [13] L. Poli, G. Oliveri, F. Viani, and A. Massa, "MT-BCS-based microwave imaging approach through minimum-norm current expansion," *IEEE Trans. Antennas Propag.*, vol. 61, no. 9, pp. 4722-4732, Sep. 2013.
- [14] N. Anselmi, G. Oliveri, M. Salucci, and A. Massa, "Wavelet-based compressive imaging of sparse targets" *IEEE Trans. Antennas Propag.*, vol. 63, no. 11, pp. 4889-4900, Nov. 2015.
- [15] N. Anselmi, G. Oliveri, M. A. Hannan, M. Salucci, and A. Massa, "Color compressive sensing imaging of arbitrary-shaped scatterers," *IEEE Trans. Microw. Theory Techn.*, vol. 65, no. 6, pp. 1986-1999, Jun. 2017.
- [16] F. Viani, G. Oliveri, and A. Massa, "Compressive sensing pattern matching techniques for synthesizing planar sparse arrays," *IEEE Trans. Antennas Propag.*, vol. 61, no. 9, pp. 4577-4587, Sept. 2013.
- [17] G. Oliveri, M. Salucci, and A. Massa, "Synthesis of modular contiguously clustered linear arrays through a sparseness-regularized solver," *IEEE Trans. Antennas Propag.*, vol. 64, no. 10, pp. 4277-4287, Oct. 2016.
- [18] P. Rocca, M. A. Hannan, M. Salucci, and A. Massa, "Single-snapshot DoA estimation in array antennas with mutual coupling through a multi-scaling BCS strategy," *IEEE Trans. Antennas Propag.*, vol. 65, no. 6, pp. 3203-3213, Jun. 2017.
- [19] P. Rocca, M. Benedetti, M. Donelli, D. Franceschini, and A. Massa, "Evolutionary optimization as applied to inverse problems," *Inverse Probl.*, vol. 25, pp. 1-41, Dec. 2009.
- [20] P. Rocca, G. Oliveri, and A. Massa, "Differential Evolution as applied to electromagnetics," *IEEE Antennas Propag. Mag.*, vol. 53, no. 1, pp. 38-49, Feb. 2011.